Temporal super-resolution in single-molecule experiments

Colin D. Kinz-Thompson and Ruben L. Gonzalez, Jr.

Department of Chemistry, Columbia University, New York, NY 10027

To whom correspondence should be addressed: cdk2119@columbia.edu (C.D.K.) and rlg2118@columbia.edu (R.L.G.)

ABSTRACT
Many time-resolved single-molecule biophysics experiments seek to characterize the kinetics of biomolecular systems exhibiting dynamics that challenge the time resolution of the given technique. Here we present a general, computational approach to this problem that employs Bayesian inference to learn the underlying dynamics of such systems, even when these kinetics are much faster than the time resolution of the given technique. By accurately and precisely inferring rate constants, this Bayesian Inference for the Analysis of Sub-temporal-resolution Data (BIASD) approach effectively enables the experimenter to super-resolve the poorly resolved, fast kinetics that are present in their data.

INTRODUCTION

Given their inherent ability to eliminate ensemble averaging, time-resolved single-molecule biophysical methods have revolutionized the study of biological mechanisms by enabling distributions of molecular properties to be observed, transiently sampled reaction intermediates to be characterized, and stochastic fluctuations from equilibrium to be investigated.[1] Despite their impact, however, these methods continue to be significantly limited by the maximum time resolutions that can be achieved while still maintaining acceptable signal-to-noise ratios (SNR) and sufficient experimental throughput (*i.e.*, observation of a statistically significant number of molecules given a feasible experimental effort).[2] Some of the most widely used single-molecule approaches, for example, including wide-field fluorescence microscopy, force spectroscopy, and tethered particle motion techniques, are typically limited to time resolutions of milliseconds to hundreds of milliseconds per data point.[3–6] Consequently, these single-molecule methods often fail to detect or properly characterize mechanistically critical biomolecular processes, such as early steps in ligand binding and/or dissociation, structural domain rearrangements, or local folding and unfolding events, that occur on the microsecond to millisecond timescale.[7,8] Although the time resolution of some single-molecule methods can be improved so that they might be able to report on these processes, such as by performing single-molecule fluorescence microscopy experiments using a confocal, rather than a wide-field, fluorescence microscope, this often comes at the cost of a significant decrease in the SNR and/or a several orders of magnitude decrease in the experimental throughput, either of which can be as powerful a limitation as the lower time resolution.[2]

To push beyond the time-resolution limits of single-molecule methods without altering SNRs or experimental throughputs, we have developed a computational approach that can infer the rate constants governing transitions between multiple ligand-binding- or conformational states (hereafter referred to just as 'states') of a single molecule from the analysis of any time-resolved, single-molecule experimental signal–even if those rates are substantially faster than the time resolution of the recorded experimental signal. Much like the

ability to infer the spatial position of a single-molecule in super-resolution imaging experiments, this approach, which we call *B*ayesian *I*nference for the *A*nalysis of *S*ub-temporal resolution *D*ynamics (BIASD), allows for temporal super-resolution in single-molecule experiments. By using Bayesian inference, BIASD also employs a natural framework with which to describe the precision that the amount of data collected during the single-molecule experiment will lend to the determination of the parameters governing the single-molecule dynamics.[9]

Here, we describe the Bayesian inference-based framework underlying BIASD. We then validate BIASD on computer-simulated data by accurately recovering the known rate constants governing transitions between states that were used to generate computer-simulated signal *versus* time trajectories (signal trajectories). Having validated BIASD, we next apply it to experimental data in order to infer the unknown rate constants governing transitions between states in experimentally recorded fluorescence resonance energy transfer efficiency (E_{FRET}) *versus* time trajectories (E_{FRET} trajectories). Notably, the experimentally recorded E_{FRET} trajectories that we have analyzed here had until now eluded analysis due to the presence of transitions that are much faster than the time resolution of the electron-multiplying charge-coupled device camera that was used to record them.[10] Finally, we describe and apply a straightforward extension of the BIASD framework that can be used to infer rate constants and signal values on experimental systems consisting of static or interconverting sub-populations of molecular properties within an individual or ensemble of molecules. Remarkably, the results of our studies demonstrate that, even when the rates of transitions between states are orders of magnitude faster than the time resolution of the signal trajectories, BIASD permits accurate inference of the rates constants for transitions between these states.

Bayesian Inference-based Framework Underlying BIASD

In biomolecular systems, functional motions—such as those involved in ligand binding and dissociation processes, or large-scale conformational rearrangements—very often involve the simultaneous formation and/or disruption of numerous, non-covalent interactions. The relatively low probability of simultaneously forming and/or disrupting these numerous interactions can therefore result in large, entropically dominated, transition-state energy barriers for such functional motions.[11,12] Consequently, individual biomolecules are generally expected to exhibit effectively discrete and instantaneous transitions between relatively long-lived states,[8] an expectation that is consistent with the step-like transitions that are generally observed in time-resolved single-molecule experiments.[13] By definition, such time-resolved single-molecule techniques record the time evolution of an experimentally observable signal originating from an individual molecule (*i.e.*, a signal trajectory) that, ideally, conveys information about the time evolution of the underlying state of that molecule. Correspondingly, the analysis of a single-molecule signal trajectory frequently involves thresholding the trajectory at particular signal values or modeling the trajectory (*e.g.*, using a hidden Markov model (HMM)) such that each data point in the signal trajectory is assigned to a single, specific state of the molecule.[14,15] As a result, these methods 'idealize' the original signal trajectory into a state *versus* time trajectory (state trajectory). From the idealized state trajectory, the distribution of dwell times spent in a particular state before undergoing a transition to another state can be used to determine the rate constants for the transitions between states, and the distribution of observed signal values originating from a particular state can be used to determine the signal value corresponding to that state.[1,16]

An important consideration when idealizing signal trajectories is that whenever an individual molecule undergoes a transition from one state to another, the transition occurs stochastically during the time period, τ, over which the detector collects and integrates the signal to record a data point in the signal trajectory. Thus, the probability that a transition will coincide exactly with the beginning or end of the τ in which it takes place is

essentially zero. As a result, when a transition takes place, the signal value that is recorded during that τ does not solely represent either of the states involved in that transition. Instead, it represents the average of the signal values corresponding to the states that are sampled during τ, weighted by the time spent in each of those states. This time averaging makes it imprudent, if not incorrect, to idealize the signal value recorded during such a τ by assigning it to any one particular state, because the molecule will have occupied multiple states during that τ. Notably, when the rates of transitions between states become comparable to or greater than τ^{-1}, there is a large probability that the τs of a signal trajectory will contain one or more transitions, and that, consequently, many of the signal values of the signal trajectory will exhibit this time averaging. Idealization of such signal trajectories, therefore, introduces significant errors into the resulting dwell-time- and signal-value distributions as well as into the rate constants for transitions between states and signal values corresponding to those states that are determined from these distributions.[9]

In order to overcome the potential errors associated with determining rates of transitions and signal values from the analysis of idealized state trajectories, BIASD instead determines the rates of transitions and signal values by analyzing the fraction of time that a molecule spends in each state during the τ corresponding to each signal value in a signal trajectory. To illustrate this approach, we consider the case of an individual molecule that undergoes stochastic and uncorrelated (*i.e.*, Markovian) and reversible transitions between two states, denoted 1 and 2, (*i.e.*, 1 $\rightleftarrows$ 2, with forward and reverse rate constants of k_1 and k_2, respectively) that have unique signal values of ϵ_1 and ϵ_2. If the fraction of time that the molecule spends in state 1 during a particular τ is f, then, because of the two-state nature of the system, the fraction of time that the molecule spends in state 2 during that τ is 1-f. It is important to note that, although the molecule is at equilibrium between states 1 and 2, the value of f for any particular τ will not necessarily be the equilibrium value of f = $(1+(k_1/k_2))^{-1}$, because τ might not be long enough for sufficient time averaging to occur (*i.e.*, to invoke ergodicity). Instead, each τ will exhibit a different, time-averaged value of f.

The exact value of f for a particular τ will depend upon the molecule's stochastic path through state-space during τ. As such, a probabilistic description of f, which accounts for all possible paths through state-space, is needed to calculate the likelihood of observing a particular value of f during a τ.[17,18] In particular, for the reversible, two-state system considered here, such a description, which has roots in nuclear magnetic resonance chemical exchange experiments,[19] and sojourn-time distributions,[20] was first given by Dobrushin;[21] in its use here, this expression depends upon k_1, k_2, and τ, and is derived in the *Supporting Information*. Experimentally, if the exact values of f, ϵ_1, and ϵ_2 during each τ were known, one would be able to calculate the expected value of the corresponding time-averaged signal, μ, for each τ because it would be the linear combination $\mu = (\epsilon_1 \cdot f) + (\epsilon_2 \cdot (1-f))$. Unfortunately, the analysis of time-resolved single-molecule experiments deals with the opposite problem—observing a signal, d, during each τ and trying to infer f, ϵ_1, and ϵ_2—with additional uncertainty that is due, in part, to noise in the measurement of d.

A conservative, yet generally applicable, approach to analyzing the value of d recorded during each τ is to treat it as a noisy measurement of μ. By assuming that detection noise (*e.g.,* readout noise) dominates over other possible sources of noise (*e.g.*, fluctuations in laser power), and that such detection noise is effectively uncorrelated, the observed values of d will have a probability that is distributed according to a normal (*i.e.,* Gaussian) distribution with a mean, μ, and a standard deviation, σ, corresponding to the amount of noise in d. However, since μ depends upon f, which is not an experimental observable, we have no way of knowing the exact value of μ during a measurement, information that would ordinarily be required to calculate the probability of observing a particular value of d. To circumvent this experimental limitation, this dependence upon f can be removed by marginalizing f out of the expression for the normal probability distribution function for d that was

described above. This marginalized probability distribution of d then describes the likelihood of experimentally observing a particular value of d during a τ as a function of the rates of transitions between the states (k_1 and k_2), the signal values corresponding to those states (ϵ_1 and ϵ_2), and the amount of noise in d (σ), regardless of the exact value of f (Fig. 1A) (See the *Supporting Information* for a full derivation of the expression describing the marginalized probability distribution of d for a two-state system).

With such an expression describing the marginalized probability distribution of d, we can then use Bayesian inference to estimate the model parameters governing the kinetics of the single-molecule system (*i.e.*, k_1, k_2, ϵ_1, ϵ_2, and σ) from the series of the d_i that comprise each of the signal trajectories. Primarily due to recent developments in computational tractability, Bayesian inference has become a powerful method for the analysis of biophysical data, such as determining the phases of X-ray reflections in X-ray crystallographic studies,[22] performing simultaneous phylogenetic analysis of nucleotide and protein datasets,[23] elucidating the number of structural classes present in cryogenic electron microscopy images,[24] and ascertaining the number of states and the rates of transitions between those states present in single-molecule signal trajectories.[25,26] For a practical introduction to Bayesian inference, see Refs. 27 and 28, and the *Supporting Information*. Unfortunately, performing Bayesian inference on a multi-parameter system, such as the one described here, results in a multi-dimensional, joint-probability distribution of the model parameters known as a posterior probability distribution, which is difficult to evaluate.[27] In order to overcome this difficulty, we evaluate the posterior distribution of the model parameters by numerically sampling it using a Markov chain Monte Carlo (MCMC)[28,29] method with affine-invariant ensemble sampling.[30,31] Although alternative methods that approximate the posterior distribution of the model parameters, such as the Laplace approximation or variational inference, might be more computationally tractable, MCMC sampling is advantageous in that, unlike such approximation methods, it can provide an exact result that does not assume a particular structure of the posterior.[28] Regardless of the choice of method, however, the most important aspect of the approach described here is that we can evaluate or estimate the posterior distribution of the model parameters from the series of d_i that comprise a single-molecule signal trajectory in a manner that completely accounts for the time resolution of the trajectory.

RESULTS AND DISCUSSION

Analysis of Computer-Simulated Single-Molecule Signal Trajectories Reporting on the Kinetics of a Ligand Binding and Dissociation Process

To validate BIASD, we simulated single-molecule signal trajectories that mimic the binding and dissociation of a ligand to its target biomolecule, a receptor, using the two-state, reversible kinetic scheme discussed in the previous section.[32] In this example, ϵ_1 and ϵ_2 represent the signal values of the receptor in the ligand-free state, and the ligand-bound state, respectively. Correspondingly, k_1 and k_2 represent the pseudo-first-order rate constant of ligand binding to the receptor, and the first-order rate constant of ligand dissociation from the receptor, respectively. As such, the concentration-dependence of k_1 is given by $k_1 = k_1^* \cdot [L]$, where k_1^* is the second-order rate constant for binding of the ligand to the receptor, and [L] is the ligand concentration; k_2 is not dependent on [L]. In order to emulate a titration experiment, we varied the [L] to alter the fraction of ligand-bound receptor from ~0.1% to ~99.9%, and simulated signal trajectories where the [L] spanned six decades centered around the equilibrium dissociation constant, [L] = K_D.

For these simulations of a ligand-receptor system, we chose to use parameters that are consistent with total internal reflection fluorescence (TIRF) microscope smFRET experiments. As such, we chose $k_2 = \tau^{-1} = 10$ sec^{-1}, because $\tau = 0.1$ sec is typical of many smFRET experiments, and in this rate constant regime, the

process of idealizing signal trajectories into state trajectories yields many missed events, which introduces errors into the analysis of rate constants and signal values.[9] Moreover, we chose k_1^* to be 10 μM^{-1} sec^{-1} in order to yield an equilibrium dissociation constant of $K_D = 1$ μM for this simulated system, which is typical of many naturally occurring, weakly interacting, ligand-receptor systems.[2] Time-averaged signal trajectories were generated by using values of $\epsilon_1 = 0.0$, $\epsilon_2 = 1.0$, and $\sigma = 0.04$; these values are typical of experimental E_{FRET} trajectories recorded using a wide-field, TIRF microscope. Notably, each signal trajectory was simulated for 1000 data points to be consistent with a typical length of time that single-molecule E_{FRET} trajectories can be recorded before fluorophore photobleaching terminates data collection; this creates an intrinsic limitation to the amount of kinetic information contained in each signal trajectory. Finally, all of these simulated signal trajectories were then analyzed using both threshold-based idealization and using BIASD in order to obtain estimates of the underlying simulation parameters; HMM-based idealization methods provide similar results to threshold-based idealization (data not shown).

As shown in Figure 2, the values of k_1 and k_2 obtained using idealization-based methods are highly inaccurate. The traditional (maximum-likelihood) estimates of the rate constants[9] are not even defined for many of the [L]s, because no transitions occurred and/or were observed during the finite length of those signal trajectories. Notably, using a Bayesian approach to calculate the rate constants from the idealized signal trajectories at least allows rate constants to be defined across the entire span of [L].[9] Regardless, these rate constants were systematically underestimated by idealization-based methods across nearly the entire range of [L]s that were simulated, and this underestimation worsens with increasing [L]. Notably, the values of k_1 and k_2 obtained using these methods are also relatively precise–a misleading consequence of using these methods.[9]

With regard to the values of ϵ_1 and ϵ_2 obtained using idealization-based methods, Figure 2B demonstrates that, while these methods can accurately determine the value of ϵ_1 if the receptor preferentially occupies the ligand-free state (low [L]) or ϵ_2 if the receptor preferentially occupies the ligand-bound state (high [L]), the time averaging caused by fast values of k_1 shift the inferred value of ϵ_1, sometimes quite significantly, toward the simulated value of ϵ_2, and *vice versa.* Additionally, we note that for the fastest values of k_1, idealizing the signal trajectories resulted in no data points being assigned to the ligand-free state, and thus no estimate of ϵ_1 could even be made.

In contrast to the idealization-based methods, the values of k_1 and k_2 obtained using BIASD are highly accurate (Fig. 2). The simulated values of k_1 and k_2 are well encompassed by the posterior probability distribution across the entire range of [L]s that were simulated, which includes rate constants that are three orders of magnitude greater than the simulated time resolution. In addition, these results are remarkably precise, as the posterior probability distributions are strikingly narrow over a range of [L]s that corresponds to k_1 being over an order of magnitude slower to over an order of magnitude faster than τ^{-1}. Importantly, the results are relatively insensitive to the prior probability distributions that BIASD uses for the analysis (*i.e.*, the initial knowledge of k_1, k_2, ϵ_1, ϵ_2, and σ) (data not shown).

At the lower [L]s, the broadening of the posterior probability distribution that limits the precision for the estimates of k_1 and k_2 in both BIASD as well as the Bayesian transition probability method arises from the finite amount of information regarding k_2 and, to a lesser extent, ϵ_2 that is contained in signal trajectories that, at these [L]s, exhibit very low occupation of the ligand-bound state of the receptor. Likewise, at the higher [L]s, the broadening of the posterior probability distribution and the implied limitations to the precision for estimating k_1 and k_2 that is observed arises from the finite amount of information regarding k_1 and ϵ_1 that is contained in signal trajectories that, at these [L]s, exhibit very little occupation of the ligand-free state of the receptor. As a consequence of this finite amount of information, many reciprocal pairs of k_1 and ϵ_1 values (*i.e.,* a faster k_1 and

a smaller ϵ_1, or a slower k_1 and a larger ϵ_1) can be consistent with the data. In an experimental situation, this imprecision can be alleviated by employing stronger prior probability distributions for the ϵ values using the results of experiments performed under conditions in which one or the other state is preferentially occupied, for instance, in the absence of ligand or in the presence of saturating [L]. In the case of large-scale conformational rearrangements, one could similarly use a buffer condition, ligand, temperature, or mutation that preferentially stabilizes one or the other state, or, alternatively, one could use molecular structures or modeling to estimate distributions of ϵ values.

With regard to the values of ϵ_1 and ϵ_2 obtained using BIASD, Figure 2B demonstrates that these values were accurately inferred regardless of the value of [L], even when the idealization-based methods drastically misestimate these values. Moreover, ϵ_1 and ϵ_2 were inferred with high precision across all values of [L]. Finally, unlike the maximum-likelihood approach, which was only able to successfully infer σ when the signal trajectories were almost entirely in the ligand-bound or ligand-free states, BIASD was also able to accurately and precisely infer σ from all of the simulated signal trajectories (Fig. 2C).

In summary, we were able to use BIASD to obtain accurate and precise posterior probability distributions for k_1, k_2, ϵ_1, ϵ_2, and σ across the entire range of [L]s that were simulated. Notably, BIASD was even successful when the rate constants in the simulated, single-molecule signal trajectories were much slower then τ^{-1}, although we note that, in this regime, the conventional analysis of idealizing the signal trajectories is much more computationally efficient. Most importantly, BIASD was able to accurately and precisely infer the rates constants and the signal values for simulated, single-molecule signal trajectories in which the rate constants were three orders of magnitude faster than τ^{-1} and about four orders of magnitude faster than that where conventional idealization of signal trajectories begins to yield significant errors in the rate constants.

Analysis of Experimentally Observed Single-Molecule E_{FRET} Trajectories Reporting on the Kinetics of a Large-Scale Conformational Rearrangement

To demonstrate the utility of BIASD in the analysis of experimental data, we chose to analyze experimentally observed, single-molecule E_{FRET} trajectories reporting on a large-scale conformational rearrangement of the ribosome. This essential, two-subunit, ribonucleoprotein-based, biomolecular machine is universally responsible for the synthesis of proteins in living cells, which is a process known as translation. The ribosome synthesizes proteins by repeatedly incorporating amino acids, delivered in the form of aminoacyl-transfer RNA (tRNA) substrates, into a nascent polypeptide chain in the order dictated by the messenger RNA being translated. During the elongation stage of protein synthesis,[33] the ribosomal pre-translocation (PRE) complex undergoes stochastic, thermally driven fluctuations between two major, on-pathway conformational states that we refer to as global state 1 (GS1) and global state 2 (GS2), defining a dynamic equilibrium, GS1⇌GS2.[3,4] These transitions between GS1 and GS2 constitute large-scale rearrangements of the PRE complex that involve relative rotations of the ribosomal subunits, reconfigurations of the ribosome-bound tRNAs, and repositionings of a ribosomal structural domain known as the L1 stalk (Fig. 3A).[34]

Previously, we have conducted wide-field, TIRF microscopy smFRET studies of the temperature dependence of the rate constants governing GS1→GS2 and GS2→GS1 transitions by imaging a Cyanine 3 (Cy3) FRET donor fluorophore- and Cyanine 5 (Cy5) FRET acceptor fluorophore-labeled PRE complex analog lacking a tRNA at the ribosomal aminoacyl-tRNA binding (A) site (PRE^{-A}) in a temperature-controlled, microfluidic, TIRF observation flowcell.[10] Unfortunately, the increase in thermal energy that accompanied the increasing temperature caused the rate constants for the transitions between GS1 and GS2 to increase such

6

that, at the highest temperatures, the E_{FRET} trajectories contained a significant number of time-averaged data points (Fig. S1). Regrettably, the time averaging in these E_{FRET} trajectories precluded accurate determination of the rate constants, and, correspondingly, an analysis of the thermodynamic properties of the transition-state energy barriers that control the GS1→GS2 and GS2→GS1 conformational rearrangements.[10] To overcome these limitations, we have used BIASD to analyze the sets of E_{FRET} trajectories of PRE^{-A} complexes that we have previously collected at 22, 25, 28, 31, 34, and 37 °C.[10] Here, we assume that the GS1⇌GS2 equilibrium can be represented by the reversible, two-state kinetic scheme discussed earlier. In this kinetic scheme, k_{GS1} and k_{GS2} represent the rate constants for the GS1→GS2 and GS2→GS1 conformational rearrangements, respectively. Correspondingly, ϵ_{GS1} and ϵ_{GS2} represent the E_{FRET} values of GS1 and GS2, respectively. Using this approach, all six sets of E_{FRET} trajectories were analyzed using BIASD to provide estimates of k_{GS1}, k_{GS2}, ϵ_{GS1}, ϵ_{GS2}, and σ at each temperature. Unfortunately, we cannot speak to the accuracy of results obtained through the analysis of experimental, as opposed to computer-simulated, data. However, the values of k_{GS1} and k_{GS2} that were inferred using BIASD increase monotonically with temperature (Fig. 3B), and, at the highest temperatures, were greater than 1/10th of τ^{-1} – the regime where idealization-based methods begin to systematically underestimate rate constants. Additionally, we note that the posterior probability distributions of ϵ_{GS1} and ϵ_{GS2} inferred using BIASD have means of 0.13 and 0.78, respectively, which are values of ϵ_{GS1} and ϵ_{GS2} that very closely match the values of the mean E_{FRET} of GS1 and GS2 reported in previous, room-temperature studies of the analogous PRE^{-A} complex (0.16 and 0.76, respectively).[35] This correspondence strongly suggests that the values of ϵ_{GS1} and ϵ_{GS2} obtained here using BIASD are accurate, regardless of the time averaging of the E_{FRET} trajectories recorded at the highest temperatures.

With the inferred values of k_{GS1} and k_{GS2} as a function of temperature, we then used transition-state theory to quantify the apparent transition-state energy barriers along the apparent GS1→GS2 and GS2→GS1 reaction coordinates.[36–39] Kramers' barrier-crossing theory, which was developed to analyze thermally activated, condensed-phase transitions of a Brownian particle[37–39] and is increasingly being used to analyze the conformational dynamics and folding of small, globular proteins,[13,40] may ultimately provide a more exact analysis of the apparent transition-state energy barriers along the apparent GS1→GS2 and GS2→GS1 reaction coordinates. However, its application requires knowledge regarding the viscosity of the aqueous buffer in which the PRE^{-A} complex is dissolved and the 'internal friction' of the PRE^{-A} complex that are unavailable in the current study.[13,41] As such, we have opted to use transition-state theory, and regard the results as upper limits on the apparent transition-state energy barriers along the apparent GS1→GS2 and GS2→GS1 reaction coordinates that do not account for internal friction or transition-state recrossings. To apply transition-state theory, we fit the mean rate constants at each temperature to the equation $k_{TST} = (\kappa k_B T/\hbar) \exp(-(\Delta H^{\ddagger} - T\Delta S^{\ddagger})/(k_B T))$, where κ is the transmission coefficient and is taken to be unity, k_B is the Boltzman constant, $\hbar$ is Planck's constant, and $\Delta H^{\ddagger}$ and $\Delta S^{\ddagger}$ are the enthalpic and entropic differences between the transition and ground states, which are associated with the temperature-dependent- and temperature-independent contributions to the rate constants, respectively (Fig. 3B). The results of these fits for the GS1→GS2 transition are $\Delta H^{\ddagger}_{GS1}$ = 14.3 ± 1.7 kcal mol^{-1} (±1σ) and $\Delta S^{\ddagger}_{GS1}$ = −9.9 ± 5.6 cal mol^{-1} K^{-1} (±1σ), and for the GS2→GS1 transition are $\Delta H^{\ddagger}_{GS2}$ = 13.5 ± 1.6 kcal mol^{-1} and $\Delta S^{\ddagger}_{GS2}$ = −11.8 ± 5.4 cal mol^{-1} K^{-1}. Unfortunately, a structure-based interpretation of the absolute $\Delta H^{\ddagger}$ and $\Delta S^{\ddagger}$ values for the GS1→GS2 and GS2→GS1 transitions of a single PRE^{-A} complex is significantly complicated by the complexity of the enthalpic and entropic changes that are associated with conformational rearrangements of large macromolecular complexes and the inherent limitations of transition-state theory.[8,36,42] Nonetheless, structure-based interpretations of the relative changes of the $\Delta H^{\ddagger}$s and $\Delta S^{\ddagger}$s ($\Delta\Delta H^{\ddagger}$s and $\Delta\Delta S^{\ddagger}$s) between different pairs of PRE^{-A} complexes (*e.g.*, containing

different tRNAs at the peptidyl-tRNA binding (P) site; containing wildtype or mutant P-site tRNAs; consisting of wildtype or mutant ribosomes; *etc.*) are much more straightforward and can reveal the thermodynamic contributions that particular structural features of tRNAs or ribosomes make to the apparent transition-state energy barriers along the apparent GS1→GS2 and GS2→GS1 reaction coordinates. Combined with the temperature-controlled, single-moleuce TIRF microscopy platform that we have previously described,[10] the analytical framework presented in this section now enables the collection, analysis, and interpretation of such data.

Inferring rate constants and signal values from systems with sub-populations of molecular properties

BIASD can be easily extended to address the presence of multiple, time-averaged sub-populations of molecular properties. These sub-populations may be static or interconvert, and may be present in an individual molecule or found among an ensemble of molecules. In such a situation, we can classify each data point as belonging to one of K different types of time-averaged sub-populations, and then use a '1-of-K' vector, $\vec{z}_{ij}$, to denote to which of the K sub-populations the ith data point from the jth molecule belongs. Given the one particular sub-population specified by $\vec{z}_{ij}$, the likelihood of this data point being described by the parameters of this sub-population is calculated as described above for the case of the time-averaged, single-population system. Unfortunately, in an experimental situation there is no way of knowing which sub-population a particular data point belongs to, thereby preventing the likelihood of this data point from being evaluated; this situation is similar to that of the unknown fractional occupancy, f, described above.

To address this shortcoming, we could try to infer the value of $\vec{z}_{ij}$ along with all of the other BIASD model parameters for each data point, but this is an unreasonable number of variables for an inference procedure. Additionally, we are often not concerned with the exact values of $\vec{z}_{ij}$, so much as with the occupancies of the K states (*e.g.*, steady-state occupation probabilities) or with the rate constants that describe transitions between the K states. Fortunately, instead of performing inference to learn the model parameters and the set of $\vec{z}_{ij}$s, $\{\vec{z}_{ij}\}$, we can marginalize out all of the $\{\vec{z}_{ij}\}$ by using expressions for the probabilities of each $\vec{z}_{ij}$. For instance, in the case of a mixture of static sub-populations of molecular properties among an ensemble of molecules (e.g., a mixture of post-translationally modified and unmodified molecules within an ensemble), these probabilities would be time-independent variables that specify the fraction of each sub-population of the ensemble; this approach is called a mixture model. Marginalization would then involve summing the likelihoods for the different sub-populations, weighted by the probabilities of those sub-populations. Consequently, during the inference procedure, the probabilities of the sub-populations would then become model parameters that are also inferred using Bayes' rule.

Additionally, it is possible to have a time-dependent system with hierarchical transitions between the different sub-populations. In this case, the probabilities of each $\vec{z}_{ij}$ in the $\{\vec{z}_{ij}\}$ would not be constant for each sub-population, as they would be for a mixture model, but would instead depend upon the sub-population of the previous data point $\vec{z}_{i-1,j}$ and a K x K transition matrix, $\mathbf{A}_{ij} = e^{\mathbf{Q}t_{ij}}$, where $\mathbf{Q}$ is the rate matrix that depends upon the set of rate constants for transitioning between the K different states and t_{ij} is the time that has elapsed since the previous data point, which may not necessarily be equal to τ (Fig. 1B). Here, marginalization is efficiently performed with the forward-backward algorithm[43] and the state probabilities, as calculated from the rate constants for the kinetic scheme under consideration, for instance using the diagram method,[44] are used to set the initial probability of each $\vec{z}_{0j}$. In total, this approach amounts to a hierarchical, continuous-time,

ensemble HMM for sub-temporal resolution systems, where inference is performed directly upon the rate constants, instead of the transition probabilities. Consequently, this approach can handle shuttering of the laser light source in TIRF microscopy experiments or other types of irregular spacing of data points, sub-temporal resolution data, and population-level analyses with non-parametric posterior distributions that can be used to ascertain the underlying thermodynamic landscape of the mesoscopic ensemble.

To highlight this hierarchical approach, consider a single-molecule fluorescence microscopy experiment in which a fluorophore-labeled biomolecule transitions between two states, 1 and 2, with forward and reverse rate constants k_{12} and k_{21}, respectively (Fig. 4A). Unfortunately, such fluorescence microscopy experiments often suffer from photophysical phenomena such as fluorophore photoblinking, in which a fluorophore temporarily transitions into a 'dark', long-lived, excited molecular electronic state and thus transiently stops fluorescing, or fluorophore photobleaching, where a fluorophore that has transitioned into an excited molecular electronic state undergoes a photochemical reaction and permanently stops fluorescing.[45] Often, the transition rates into and out of the dark states responsible for photoblinking are faster than the time resolution of techniques such as wide-field TIRF microscopy. As a result, instead of detecting a steady level of fluorescence intensity from the fluorophore, sub-temporal resolution transitions between fluorescent and dark states of the fluorophore manifests as an extra, and often dominant, source of 'noise' in the single-molecule fluorescence intensity signal trajectory (Fig. 4B, inset). Intense experimental effort has gone into minimizing these photophysical effects, including the use of fluorophores, such as Cy3B, that have been chemically altered so as to minimize transitions to dark states;[46] elaborate excitation laser modulation schemes, such as triplet-state relaxation (T-Rex) and dark-state relaxation (D-Rex) schemes, that minimize transitions to higher-order dark states;[47,48] photostabilizing additives, such as Trolox, that accelerate transitions out of dark states;[49,50] and fluorophore-photostabilizer conjugates, such as Cy3- and Cy5-triplet state quencher conjugates, that accelerate transitions out of dark states.[51,52] Here, we show how extending BIASD with the hierarchical HMM described above allows us to computationally overcome these photophysical effects.

To demonstrate this ability, we simulated the kinetic scheme shown in Fig. 4A, where the afore-mentioned fluorophore-labeled biomolecule transitions between conformational states 1 and 2 with signal values of ϵ_1 and ϵ_2, respectively. However, in this simulation, both of these states can rapidly transition into and out of a photoblinked state, denoted 0 with signal value $\epsilon_0 = 0$, at rates much faster than the time resolution of the simulated data. These dynamics continue until the system eventually transitions into a photobleached state, denoted $\varnothing$ with signal value $\epsilon_\varnothing = 0$. As expected, by analyzing this simulation using this hierarchical approach, the posterior probability distribution of the parameters describing the fluorescence emission from each sub-population (ϵ_1, ϵ_2, σ, k_{10}, k_{01}, k_{20}, and k_{02}; see Fig. 1B), as well as the rate constants describing the transitions between states 1 and 2 (k_{12}, and k_{21}; see Fig. 4A), were all found both accurately and precisely (Fig. S2). To provide intuition into the power of this calculation, we also have shown the Viterbi-idealized path from the maximum *a posteriori* (MAP) estimate of the model parameters in order to present the corrected fluorescence intensity signal trajectory in the absence of photoblinking (Fig. 4B). Detection noise from the marginalized posterior distribution of σ was added to this path to show what the data would have looked like in the absence of photoblinking. Regardless, we note that this path is essentially a point estimate of the $\{\vec{z}_{ij}\}$, whereas, by marginalizing out all of the $\{\vec{z}_{ij}\}$ during the inference procedure, we have actually considered all the other possible paths. As such, the posterior probability distribution of the model parameters is a more encompassing result (Fig. S2). Finally, we note that the hierarchical HMM treatment that we present here is general and applicable to not just two, but to any number of K sub-populations.

CONCLUSION

By analyzing the fraction of time that a single-molecule spends in each state of a defined kinetic scheme as well as the signal value corresponding to each of those states during each τ in a signal trajectory, BIASD adopts a fundamentally different approach to the analysis of time-resolved single-molecule experiments than that which has been traditionally employed by methods that idealize the trajectories (*e.g.*, thresholding and HMMs). Using computer-simulated and experimentally observed data, we have demonstrated that this powerful approach enables BIASD to accurately and precisely infer the rate constants of a two-state kinetic scheme as well as the signal values corresponding to these two states, even when the rates of transitions between the states are orders of magnitude faster than the time resolution of the signal trajectories. When used to analyze previously described experimental E_{FRET} trajectories reporting on the dynamics of single PRE^{-A} complexes recorded as a function of temperature,[10] BIASD allowed us to infer the thermodynamic activation parameters characterizing the transition-state energy barriers along the GS1→GS2 and GS2→GS1 reaction coordinates, which had thus far remained inaccessible to traditional smFRET data analysis approaches. Moreover, we have demonstrated that a straightforward extension of the BIASD framework enables the kinetics of experimental systems exhibiting multiple sub-populations of molecular properties to be accurately and precisely inferred.

It is important to note that the BIASD framework is general and can be applied to any experimentally observed signal trajectory that exhibits stochastic transitions between distinct states, regardless of the nature or the origin of the signal. Thus, BIASD can be used to temporally super-resolve data collected using virtually any time-resolved single-molecule experimental method, including single-molecule fluorescence microscopy, force spectroscopy, conductance, and tethered particle motion methods. Moreover, although here we have developed BIASD to analyze single-molecule signal trajectories, BIASD does not consider the temporal ordering of the data. Consequently, in addition to analyzing individual single-molecule signal trajectories, BIASD can also be used to analyze the distribution of fractional occupancies observed across an entire ensemble of individual molecules during a given τ. This could allow non-equilibrium phenomenon to be monitored across an ensemble of single molecules (*e.g.*, stopped-flow delivery of a ligand, substrate, cofactor, or inhibitor to an enzyme or other biomolecule). In addition, BIASD can be expanded to include the time evolution of the state occupation probabilities (*c.f.,* Eq. 2 of the *Supporting Information*), or to incorporate time dependence into the model parameters k_i, ϵ_i, and σ (*e.g.*, the varying of ϵ_i in single-molecule particle tracking experiments).

Regarding the performance of BIASD on experimental data, we note that the rate constants and signal values of a system can be more precisely inferred from experiments that collect higher SNR data, because then there is less uncertainty in the time-averaged fractional occupancies of the signal trajectories. Therefore, somewhat counterintuitively, sub-temporal-resolution dynamics can, to some degree, be more precisely inferred from signal trajectories recorded with lower time resolutions, but higher SNRs (*e.g.,* due to better photon conversion efficiencies on an electron-multiplying charge-coupled device), than those recorded with higher time resolutions, but lower SNRs. Additionally, although we have focused the current work on the most widely applicable case of a Markovian, two-state system in which the noise of the signal can be modeled using a Gaussian distribution, the Bayesian inference-based framework underlying BIASD can be readily extended to non-Markovian dynamics,[19,53] N-state kinetic schemes,[54,55] or systems in which the noise of the signal can be modeled using distributions other than a Gaussian distribution.[56,57] To facilitate the analysis of single-molecule data using BIASD, as well as to enable the future extension of BIASD along the lines described here, we have

made the BIASD source code available at https://github.com/ckinzthompson/biasd. The source code is written in Python and integrated with computationally intensive functions provided in C as well as in CUDA (for GPU-based computation) in order to balance accessibility with high-performance.

MATERIALS AND METHODS

Simulating Sub-temporal-resolution Signal Trajectories

To simulate state trajectories with the stochastic simulation algorithm,[32] sequential random lifetimes were drawn from exponential distributions with the appropriate rate constants, and subsequent states were chosen randomly according to the splitting probabilities. A random starting point for the initiation of the trajectory (t=0 sec) was selected with a uniform distribution from the first lifetime. The fractional occupancies of each state during each sequential τ were then calculated from the sequence of lifetimes. The resulting fractional occupation *versus* time trajectories were turned into signal trajectories by computing μ, and then adding normally distributed noise with standard deviation, σ.

Idealizing Trajectories

Signal trajectories were idealized by thresholding any measurement period with signal less than (ϵ_2 - ϵ_1)/2 + ϵ_1 into state 1, and otherwise into state 2. Rate constants from the ith state to j^{th} state were then calculated from the resulting transition matrix, p_{ij}, as k_{ij} = -ln(1-p_{ij})/τ.[9] Credible intervals on the transition probabilities, and rate constants were calculated with uniform prior distributions.[9]

BIASD Calculations

The adaptive Simpson method was used to numerically integrate the BIASD likelihood function on an Nvidia GeForce GTX 750 Ti graphics card; the likelihood of each data point took about 1 μs to compute. The posterior probability distribution was sampled using emcee, an ensemble, affine-invariant MCMC method.[30,31] For each trajectory, 100 MCMC walkers were employed to draw 2000 samples each, and the first 1000 samples were discarded to burn in the chain. From the remaining samples, independent samples were chosen spaced apart by the maximum parameter autocorrelation time, and credible intervals and means were calculated from these samples.

Processing PRE^{-A} E$_{FRET}$ Data

Previously published Cy3 and Cy5 fluorescence intensity, I_{Cy3} and I_{Cy5}, *versus* time trajectories from the PRE^{-A} complex from the study by Wang and coworkers[10] were transformed into E$_{FRET}$ trajectories by calculating $E_{FRET} = I_{Cy5}/(I_{Cy3} + I_{Cy5})$ at each measurement period. Outliers where $E_{FRET} < -0.4$ or $E_{FRET} > 1.4$ were then removed. The number of E$_{FRET}$ trajectories retained in the 22, 25, 28, 31, 34, and 37 °C datasets were 490, 456, 435, 452, 270, and 459, respectively. Posterior probability distributions were found with the Laplace approximation of the BIASD likelihood function, and used to set the means of the prior probability distributions employed for ϵ_{GS1}, ϵ_{GS2}, and σ (normal distribution, normal distribution, and gamma distribution, respectively). The prior probability distributions for k_{GS1} and k_{GS2} were both taken to be gamma distributions with a mean determined from the Laplace approximation solution, and shape parameter $\alpha = 1$ to ensure a weakly-informative prior.

ACKNOWLEDGEMENTS

REFERENCES

1. Tinoco, I. & Gonzalez, R. L. Biological mechanisms, one molecule at a time. *Genes Dev.* **25,** 1205–1231 (2011).
2. Kinz-Thompson, C. D. & Gonzalez, R. L. smFRET studies of the 'encounter' complexes and subsequent intermediate states that regulate the selectivity of ligand binding. *FEBS Lett.* **588,** 3526–38 (2014).
3. Fei, J., Kosuri, P., MacDougall, D. D. & Gonzalez, R. L. Coupling of ribosomal L1 stalk and tRNA dynamics during translation elongation. *Mol. Cell* **30,** 348–59 (2008).
4. Fei, J. *et al.* Allosteric collaboration between elongation factor G and the ribosomal L1 stalk directs tRNA movements during translation. *Proc. Natl. Acad. Sci.* **106,** 15702–7 (2009).
5. Greenleaf, W. J., Frieda, K. L., Foster, D. A. N., Woodside, M. T. & Block, S. M. Direct Observation of Hierarchical Folding in Single Riboswitch Aptamers. *Science* **319,** 630–633 (2008).
6. Schafer, D. A., Gelles, J., Sheetz, M. P. & Landick, R. Transcription by single molecules of RNA polymerase observed by light microscopy. *Nature* **352,** 444–448 (1991).
7. Boehr, D. D., Dyson, H. J. & Wright, P. E. An NMR perspective on enzyme dynamics. *Chem. Rev.* **106,** 3055–3079 (2006).
8. McCammon, J. A. Protein dynamics. *Reports Prog. Phys.* **47,** 1–46 (1984).
9. Kinz-Thompson, C. D., Bailey, N. A. & Gonzalez, R. L. in *Methods in enzymology* **581,** 187–225 (2016).
10. Wang, B., Ho, J., Fei, J., Gonzalez, R. L. & Lin, Q. A microfluidic approach for investigating the temperature dependence of biomolecular activity with single-molecule resolution. *Lab Chip* **11,** 274–81 (2011).
11. Fenimore, P. W., Frauenfelder, H., McMahon, B. H. & Parak, F. G. Slaving: solvent fluctuations dominate protein dynamics and functions. *Proc. Natl. Acad. Sci.* **99,** 16047–16051 (2002).
12. Lubchenko, V., Wolynes, P. G. & Frauenfelder, H. Mosaic energy landscapes of liquids and the control of protein conformational dynamics by glass-forming solvents. *J. Phys. Chem. B* **109,** 7488–7499 (2005).
13. Chung, H. S. & Eaton, W. a. Single-molecule fluorescence probes dynamics of barrier crossing. *Nature* **502,** 685–8 (2013).
14. Chung, S. H., Moore, J. B., Xia, L. G., Premkumar, L. S. & Gage, P. W. Characterization of single channel currents using digital signal processing techniques based on Hidden Markov Models. *Philos. Trans. R. Soc. Lond. B. Biol. Sci.* **329,** 265–85 (1990).
15. Qin, F., Auerbach, a & Sachs, F. A direct optimization approach to hidden Markov modeling for single channel kinetics. *Biophys. J.* **79,** 1915–1927 (2000).
16. Colquhoun, D. & Hawkes, A. G. On the stochastic properties of single ion channels. *Proc. R. Soc. London. Ser. B* **211,** 205–235 (1981).
17. Flomenbom, O. & Silbey, R. J. Path-probability density functions for semi-Markovian random walks. *Phys. Rev. E - Stat. Nonlinear, Soft Matter Phys.* **76,** 1–5 (2007).
18. Hanson, J. a *et al.* Illuminating the mechanistic roles of enzyme conformational dynamics. *Proc. Natl. Acad. Sci.* **104,** 18055–60 (2007).
19. Berezhkovskii, A. M., Szabo, A. & Weiss, G. H. Theory of single-molecule fluorescence spectroscopy of two-state systems. *J. Chem. Phys.* **110,** 9145 (1999).
20. Good, I. The Frequency Count of a Markov Chain and the Transition to Continuous Time. *Ann. Math. Stat.* **32,** 41–48 (1961).

21. Dobrushin, R. Limit theorems for a markov chain of two states. *Izv. Ross. Akad. Nauk. USSR Seriya Mat.* **17,** 291–330 (1953).

22. Gilmore, C. J. Maximum Entropy and Bayesian Statistics in Crystallography: a Review of Practical Applications. *Acta Crystallogr. Sect. A Found. Crystallogr.* **52,** 561–589 (1996).

23. Ronquist, F. & Huelsenbeck, J. P. MrBayes 3: Bayesian phylogenetic inference under mixed models. *Bioinformatics* **19,** 1572–1574 (2003).

24. Scheres, S. H. W. RELION: Implementation of a Bayesian approach to cryo-EM structure determination. *J. Struct. Biol.* **180,** 519–530 (2012).

25. Bronson, J. E., Fei, J., Hofman, J. M., Gonzalez, R. L. & Wiggins, C. H. Learning rates and states from biophysical time series: a Bayesian approach to model selection and single-molecule FRET data. *Biophys. J.* **97,** 3196–205 (2009).

26. van de Meent, J.-W., Bronson, J. E., Wiggins, C. H. & Gonzalez, R. L. Empirical Bayes Methods Enable Advanced Population-Level Analyses of Single-Molecule FRET Experiments. *Biophys. J.* **106,** 1327–1337 (2014).

27. Sivia, D. S. & Skilling, J. *Data Analysis: A Bayesian Tutorial.* (Oxford University Press, 2006).

28. Bishop, C. M. *Pattern Recognition and Machine Learning.* (Springer, 2006).

29. Metropolis, N., Rosenbluth, A. W., Rosenbluth, M. N., Teller, A. H. & Teller, E. Equation of State Calculations by Fast Computing Machines. *J. Chem. Phys.* **21,** 1087 (1953).

30. Goodman, J. & Weare, J. Ensemble samplers with affine invariance. *Commun. Appl. Math. Comput. Sci.* **5,** 65–80 (2010).

31. Foreman-Mackey, D., Hogg, D. W., Lang, D. & Goodman, J. emcee : The MCMC Hammer. *Publ. Astron. Soc. Pacific* **125,** 306–312 (2013).

32. Gillespie, D. T. Exact Stochastic Simulation of Coupled Chemical Reactions. *J. Phys. Chem.* **81,** 2340–2361 (1977).

33. Voorhees, R. M. & Ramakrishnan, V. Structural basis of the translational elongation cycle. *Annu. Rev. Biochem.* **82,** 203–236 (2013).

34. Frank, J. Intermediate states during mRNA-tRNA translocation. *Curr. Opin. Struct. Biol.* **22,** 778–85 (2012).

35. Sternberg, S. H., Fei, J., Prywes, N., McGrath, K. A. & Gonzalez, R. L. Translation factors direct intrinsic ribosome dynamics during translation termination and ribosome recycling. *Nat. Struct. Mol. Biol.* **16,** 861–868 (2009).

36. Fersht, A. R. *Structure and mechanism in protein science. A guide to enzyme catalysis and protein folding.* (W.H. Freeman and Co., 1999).

37. Zwanzig, R. *Nonequilibrium Statistical Mechanics.* (Oxford University Press, 2001).

38. Van Kampen, N. G. *Stochastic Processes in Physics and Chemistry.* (North Holland, 2007).

39. Hänggi, P., Talkner, P. & Borkovec, M. Reaction-rate theory: fifty years after Kramers. *Rev. Mod. Phys.* **62,** 251–341 (1990).

40. Schuler, B., Lipman, E. a & Eaton, W. a. Probing the free-energy surface for protein folding with single-molecule fluorescence spectroscopy. *Nature* **419,** 743–747 (2002).

41. Soranno, A. *et al.* Quantifying internal friction in unfolded and intrinsically disordered proteins with single-molecule spectroscopy. *Proc. Natl. Acad. Sci.* **109,** 17800–17806 (2012).

42. Chandler, D. Statistical mechanics of isomerization dynamics in liquids and the transition state approximation. *J. Chem. Phys.* **68,** 2959 (1978).

43. Rabiner, L. R. A Tutorial on Hidden Markov Models and Selected Applications in Speech Recognition. *Proc. IEEE* **77,** 257–286 (1989).

44. Hill, T. L. *Free Energy Transduction and Biochemical Cycle Kinetics.* (Dover Publications, 2005).

45. Ha, T. & Tinnefeld, P. Photophysics of fluorescent probes for single-molecule biophysics and super-resolution imaging. *Annu. Rev. Phys. Chem.* **63,** 595–617 (2012).

46. Cooper, M. *et al.* Cy3B: improving the performance of cyanine dyes. *J. Fluoresc.* **14,** 145–50 (2004).

47. Donnert, G., Eggeling, C. & Hell, S. W. Major signal increase in fluorescence microscopy through dark-state relaxation. *Nat. Methods* **4,** 81–86 (2007).

48. Donnert, G., Eggeling, C. & Hell, S. W. Triplet-relaxation microscopy with bunched pulsed excitation. *Photochem. Photobiol. Sci.* **8,** 481–485 (2009).

49. Rasnik, I., McKinney, S. A. & Ha, T. Nonblinking and long-lasting single-molecule fluorescence imaging. *Nat. Methods* **3,** 891–3 (2006).

50. Cordes, T., Vogelsang, J. & Tinnefeld, P. On the mechanism of trolox as antiblinking and antibleaching reagent. *J. Am. Chem. Soc.* **131,** 5018–5019 (2009).

51. Altman, R. B. *et al.* Cyanine fluorophore derivatives with enhanced photostability. *Nat. Methods* **9,** 68–71 (2012).

52. van der Velde, J. H. M. *et al.* A simple and versatile design concept for fluorophore derivatives with intramolecular photostabilization. *Nat. Commun.* **7,** 10144 (2016).

53. Abate, J. & Whitt, W. A Unified Framework for Numerically Inverting Laplace Transforms. *INFORMS J. Comput.* **18,** 408–421 (2006).

54. Gibson, A. & Conolly, B. On a Three-State Sojourn Time Problem. *J. Appl. Probab.* **8,** 716–723 (1971).

55. Berezhkovskii, A. M., Szabo, A. & Weiss, G. H. Theory of the Fluorescence of Single Molecules Undergoing Multistate Conformational Dynamics. *J. Phys. Chem. B* **104,** 3776–3780 (2000).

56. Gopich, I. V. & Szabo, A. FRET efficiency distributions of multistate single molecules. *J. Phys. Chem. B* **114,** 15221–15226 (2010).

57. Gopich, I. V & Szabo, A. Theory of the energy transfer efficiency and fluorescence lifetime distribution in single-molecule FRET. *Proc. Natl. Acad. Sci.* **109,** 7747–52 (2012).
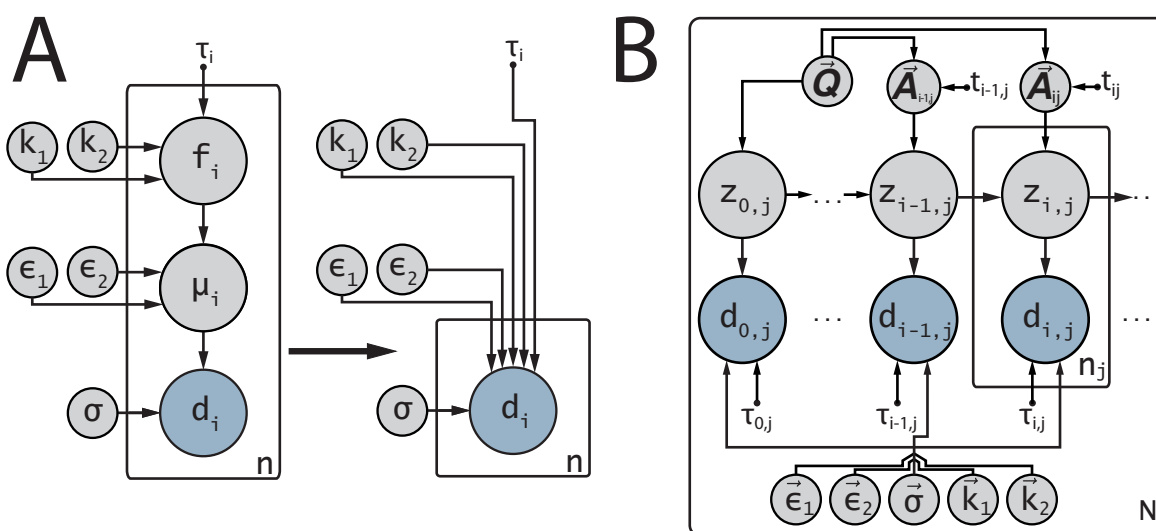
Figure 1: Graphical models for BIASD. (A) In BIASD, the dependence of the observed data, d, upon the fractional occupancy, f, is marginalized to yield the graph on right, which depends upon stochastic parameters ε_1, ε_2, σ, k_1, and k_2, as well as upon the deterministic value of τ. (B) A directed graph describing hierarchical, Markovian transitions between hidden sub-temporal-resolution sub-populations. The rate matrix, **Q**, dictates the steady state-occupation probabilities, as well as transition probabilities between sub-temporal-resolution sub-populations.
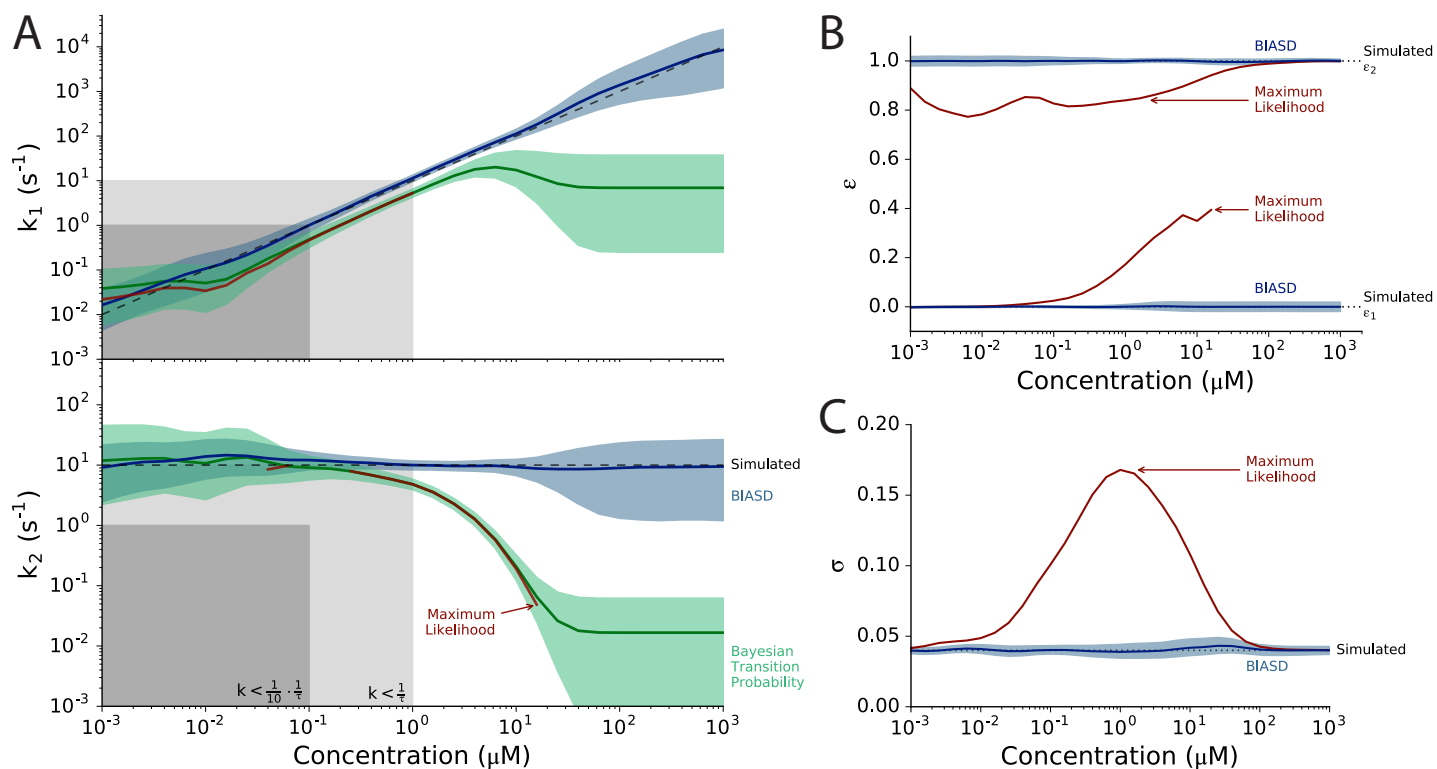
Figure 2: Analysis of k_1 and k_2 using BIASD (blue) and idealization-based (green and red) methods for a computer-simulated titration of a ligand to a receptor. [L] was varied three decades above and below the concentration where the equilibrium occupation probability of both states (K_D) is equal to 0.5. (A) Analysis of estimated rate constants k_1, and k_2. The regions where the rate constants are less than 1/10th of the acquisition rate, τ^{-1}, is shown in dark grey; the regions where the rate constants are less than the acquisition rate are shown in light grey. The simulated rate constants are plotted as the black dashed lines. The red line denotes maximum-likelihood estimate of the rate constant calculated by idealizing the signal trajectory. The green and blue areas denote the 95% credible intervals of the posterior probability distributions from analysis with idealization-based Bayesian transition probability analysis,[9] and BIASD, respectively. (B) Analysis of signal values ε_1, and ε_2. Simulated values are plotted as black dashed lines. The maximum-likelihood estimate of threshold-idealized signal trajectories is shown in red. The blue area denotes the 95% credible interval from the marginalized posterior probability distribution from BIASD. (C) Analysis of the signal noise σ. Line styles correspond to those in (B). All lines and curves were smoothed with a discrete Gaussian filter with standard deviation of 0.5 to temper variations due to the limited number of data points in each signal trajectory in order to show the general trends.
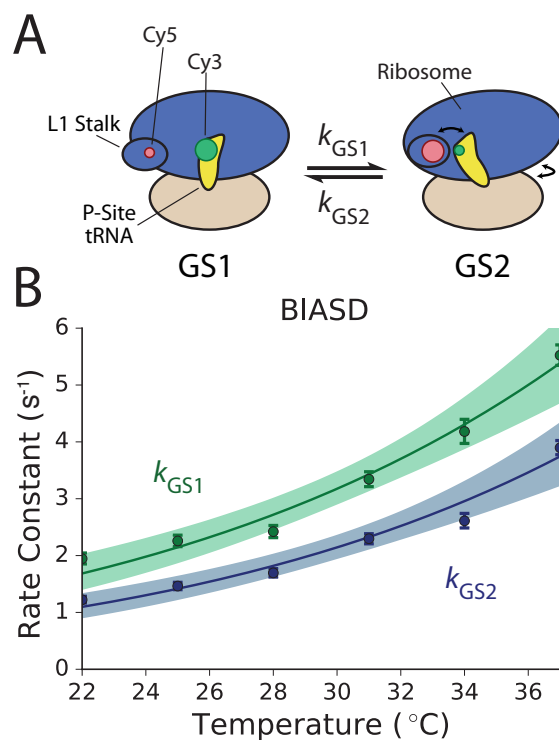
Figure 3: (A) Cartoon schematic of the GS1 ⇌ GS2 equilibrium on the PRE^{-A} complex previously studied by Wang and coworkers.[16] Approximate positions of the Cy3 FRET donor and Cy5 FRET acceptor fluorophores of the 'L1-tRNA' labeling scheme used by Wang and coworkers are shown as green and red circles, respectively. The size of the fluorophores denotes the relative fluorescence intensity of each fluorophore in each state due to FRET. (B) Temperature dependence of k_{GS1} and k_{GS2} for PRE^{-A} complexes using BIASD. The scatter plots show the expectation value of the posterior probability distributions of k_{GS1} and k_{GS2} and the error bars represent the 95% credible interval. The solid lines are the non-linear, least-squares fit to transition-state theory and the shaded regions represent 95% uncertainty from the fitting procedure.
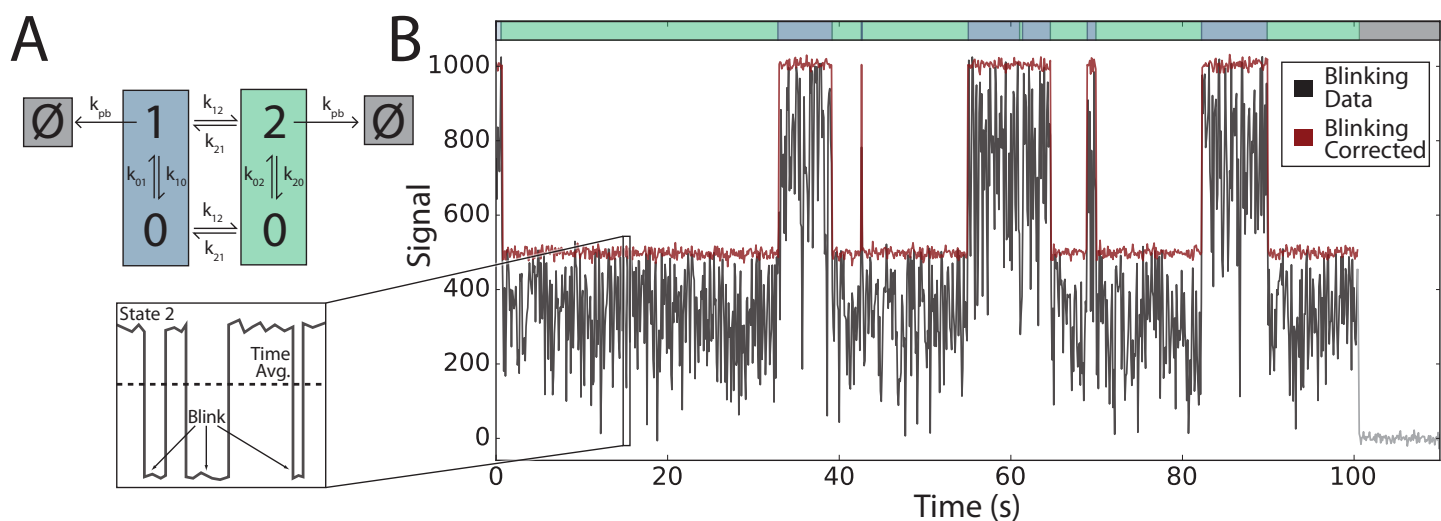
Figure 4: (A) Kinetic mechanism used to simulate an experimental system in which a biomolecule transitions between two conformational states that can each transition, with sub-temporal resolution dynamics, into and out of a photoblinked state, until eventually photobleaching. Exact values of the rate constants used in the simulation are given in the *Supporting Information*. (B) Plot of simulated signal trajectory and the resulting, corrected fluorescence intensity signal trajectory in the absence of photoblinking. The green- and blue-colored regions at the top of the plot denote the transitions between states 1 (blue) and 2 (green). The signal corrupted by sub-temporal resolution photoblinking that was analyzed by BIASD is shown in black; the inset shows a cartoon of a single τ where fast transitions are taking place between the fluorescent and photoblinked state 2. After analysis with BIASD, the MAP solution of the posterior probability distribution was used to generate a Viterbi-idealized path, which is plotted in red with noise added back from the MAP value of σ; this demonstrates what a corrected fluorescence intensity signal trajectory in the absence of photoblinking would look like.